SPE 75231

Multiple-Scale Stabilized Finite Elements for the Simulation of Tracer Injections and Waterflood

Ruben Juanes[1], SPE, and Tadeusz W. Patzek[1,2], SPE

This paper was prepared for presentation at the SPE/DOE Thirteenth Symposium on Improved Oil Recovery held in Tulsa, Oklahoma, 13-17 April 2002.

Abstract

We present a numerical method for the simulation of miscible and immiscible multiphase flow in porous media, with emphasis on the advection-dominated case. A fractional flow formulation is adopted, resulting in a "pressure" equation and a "saturation" equation. The key idea of the proposed methodology is a multiple scale decomposition of the variable of interest into resolved and unresolved scales. This acknowledges the presence of fine scales which cannot be captured by any grid, but whose influence on the coarse scales is not negligible. The multiscale approach leads to a stabilized finite element formulation, which prevents global spurious oscillations of the numerical solution without introducing excessive dissipation. The method is further improved by incorporating a novel shock-capturing technique based on a nonlinear dissipation mechanism proportional to the absolute value of the subscales. We believe this approach is entirely new in the context of flow in porous media. Numerical simulations of tracer injection (miscible flow) and waterflood (immiscible flow) are presented. The proposed subgrid scale method with shock-capturing shows exceptional performance in all test cases studied. These test cases illustrate the potential and applicability of the proposed formulation for solving multiphase compositional flows in porous media.

[1]Civil and Environmental Engineering. U.C. Berkeley.
[2]Earth Sciences Division. Lawrence Berkeley National Lab.

Introduction

The study of multiphase flow and multicomponent transport in porous and fractured media is crucial in assessing many processes relevant for improved oil recovery, such as tracer injection and flooding by water alternating gas. Quantitative prediction of these processes involves several modeling steps, shown in **Figure 1**.

There are many difficulties associated with the correct conceptualization and mathematical formulation of the problem, due to scarcity of data and the complexity of the physical processes governing flow of several phases through a porous medium. Under certain assumptions, the field-scale mathematical problem can be expressed as a set of partial differential equations with the appropriate boundary conditions, and a set of algebraic equations providing closure. In all real cases, the mathematical problem needs to be solved numerically because the nonlinearity of the equations, presence of heterogeneities and fractures, complex geometries and time-dependent boundary conditions rule out analytical solutions.

Development of novel numerical methods for the full equations of multiphase compositional flow in multidimensions must necessarily start from simplified models in one space dimension. These reduced model problems should display, however, the key features which pose difficulties in obtaining satisfactory numerical solutions such as, for instance, wild nonlinearity, shocks or near-shocks, boundary layers and degenerate diffusion. We study miscible and immiscible flow of two components. We adopt a fractional

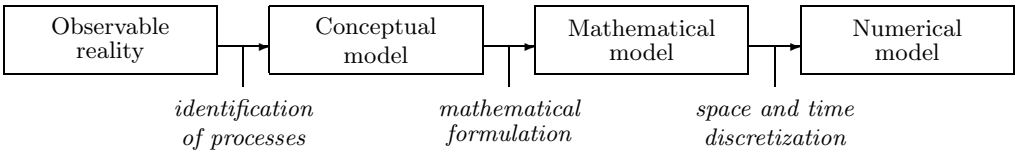

Figure 1: Steps in the development of a numerical model

flow approach,[1,2] which results in a continuity equation for the total flow ("pressure" equation) and a conservation law ("concentration" or "saturation" equation) for one of the components. The work presented here focuses on the numerical solution of the latter.

Under the assumption of incompressible fluid and rock, the "pressure" equation is of elliptic type. For its numerical solution, the current trend is to use mixed or hybrid finite element methods,[3] since they provide a better resolution of the total velocity than standard approximations.[4,5]

The "saturation" equation is a (possibly nonlinear) advection-diffusion equation. We are interested in the advection-dominated case, whose solution naturally develops sharp features. Classical numerical methods produce a solution that either lacks *stability*, resulting in nonphysical oscillations, or *accuracy*, by showing excessive numerical diffusion.

Numerical methods for the solution of the advection-diffusion equation come in two flavors:[6] Eulerian methods and characteristics methods. *Eulerian methods* discretize the equations in space using a fixed mesh, and include streamline diffusion (SD) methods[7–9] with shock-capturing,[10–18] total variation diminishing (TVD) methods,[19–23] essentially nonoscillatory (ENO) schemes[24,25] and discontinuous Galerkin (DG) methods.[9,26,27] Among *characteristics methods*, we find particle tracking,[28,29] the modified method of characteristics (MMOC),[30–32] Eulerian-Lagrangian methods[33,34] and Eulerian-Lagrangian localized adjoint methods (ELLAM).[35–40] The main idea of all characteristics methods is to split the advective and diffusive terms, adopting a Lagrangian viewpoint for the former. The splitting procedure symmetrizes and stabilizes the equations, allowing for larger time steps.[6] However, these methods rely on a good approximation of the characteristics, which requires a fine mesh for highly nonlinear problems, thus restricting severely the range of element Peclet numbers the method can handle.

Recently, stabilized methods of the streamline-upwind/Petrov-Galerkin (SUPG)[8] and Galerkin least squares (GLS)[41,42] type have been interpreted in the context of multiscale phenomena.[43–45] It is this multiscale approach that we investigate in this paper. The key point of the proposed formulation is a multiple-scale decomposition of the variable of interest into resolved (or grid) scales and unresolved (or subgrid) scales, which acknowledges the fact that the fine-scale structure of the solution cannot be captured by *any* mesh. However, the influence of the subgrid scales on the resolvable scales is not negligible. By accounting for the subgrid scales, the oscillatory behavior of classical Galerkin is drastically reduced and confined to a small neighborhood containing the sharp features, while the solution is high-order accurate where the solution is smooth. This ensures that the numerical solution is not globally deteriorated. The method does *not* emanate from a monotonicity argument and, therefore, it does not rule out small overshoots and undershoots near the sharp layers. To prevent this situation, a novel subscale-driven shock-capturing mechanism is presented. The generality of the proposed formulation makes it amenable to further extensions.

The governing equations for miscible and immmiscible flow are succinctly derived in the next section. Both the linear "concentration" equation (miscible case) and the nonlinear "saturation" equation (immiscible case) are then formulated within the unified framework of advection-diffusion conservation laws. We present the numerical formulation based on the multiple-scale approach and describe the shock-capturing technique we employed. We apply the formulation to several representative numerical simulations for both miscible and immiscible flow. In the last section we draw the main conclusions of this investigation and suggest future research.

Governing equations

In this Section we outline the derivation of the equations governing miscible and immiscible flow of two species (or components) through porous media. The basic ingredients are mass conservation of each species and a constitutive relation defining the flux of each component. A detailed derivation can be found elsewhere.[1,46,47]

Miscible flow. We consider two substances which are perfectly miscible, and assume that one is present in very small proportions. To fix ideas, we may think of a fluid mixture consisting of "dead" oil and a nonpolar tracer (see **Figure 2**).

A mass conservation statement for each species reads

$$\text{Oil:} \quad \partial_t m_o + \nabla \cdot \boldsymbol{F}_o = Q_o, \tag{1}$$

$$\text{Tracer:} \quad \partial_t m_s + \nabla \cdot \boldsymbol{F}_s = Q_s, \tag{2}$$

where m_o (resp. m_s) is the mass of oil (resp. tracer) per unit volume of porous medium, $\boldsymbol{F}_o$ (resp. $\boldsymbol{F}_s$) is the oil (resp. tracer) mass flux, and Q_o (resp. Q_s) is the oil (resp. tracer) source term. Let c be the mass fraction of tracer

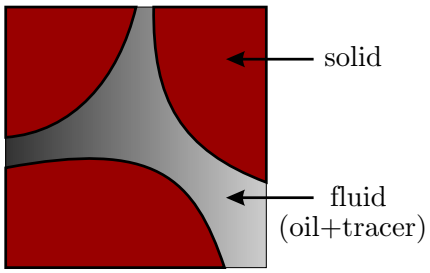

Figure 2: Schematic of miscible flow of two components in a single fluid phase

in the mixture ($c \ll 1$), we express:

$$m_o = \rho\phi(1-c), \tag{3}$$
$$m_s = \rho\phi c, \tag{4}$$

where ρ is the density of the mixture, and ϕ is the porosity of the medium. Dependence of the fluid density on the mass fraction is neglected. Similarly, we write the source term for each component as:

$$Q_o = \rho\phi q_T(1-c^*), \tag{5}$$
$$Q_s = \rho\phi q_T c^*, \tag{6}$$

where q_T is the total volumetric source of fluid, and c^* is the tracer mass fraction of the source. In the case of a negative source ($q_T < 0$), the produced fluid has a tracer mass fraction equal to that of the reservoir, i.e., $c^* = c$.

The total fluid mass flux (oil and tracer) is

$$\boldsymbol{F}_T := \boldsymbol{F}_o + \boldsymbol{F}_s = \rho\phi\boldsymbol{v}_T. \tag{7}$$

The total fluid velocity $\boldsymbol{v}_T$ is given by Darcy's law for a single-phase system (excluding gravity for expositional simplicity):

$$\boldsymbol{v}_T = -\frac{\mathbf{k}/\mu}{\phi}\nabla p, \tag{8}$$

where $\mathbf{k}$ is the absolute permeability tensor, μ is the fluid dynamic viscosity, and p is the fluid pressure.

We use an advection-diffusion formulation for the mass flux of the tracer:

$$\boldsymbol{F}_s = \rho\phi\left(\boldsymbol{v}_T c - \mathbf{D}\nabla c\right), \tag{9}$$

where $\mathbf{D}$ is the diffusion tensor, which includes the effects of molecular diffusion and hydrodynamic dispersion.[48] We assume it is independent of the mass fraction c.

Assuming incompressibility of the fluid and the medium, addition of equations (1) and (2) yields the continuity (or "pressure") equation:

$$\nabla\cdot\boldsymbol{v}_T = q_T, \tag{10}$$

where the total velocity is given by Equation (8). This is an elliptic equation, to be solved for the pressure p and the total velocity $\boldsymbol{v}_T$.

Substituting Equation (9) in (2) we obtain the mass fraction (or "concentration") equation:

$$\partial_t c + \nabla\cdot\left(\boldsymbol{v}_T c - \mathbf{D}\nabla c\right) = q_T c^*. \tag{11}$$

This is a conservation law of advection-diffusion type, to be solved for the mass fraction c. Equations (10) and (11) are decoupled and linear.

Immiscible flow. We study now the case of two fluids which are perfectly immiscible. The system involves simultaneous flow of two separate phases: the wetting phase (water) and the nonwetting phase (oil). A schematic of this situation is represented in **Figure 3**.

Using the same notation as for the miscible case, the mass conservation equations for each component are

$$\text{Oil:}\quad \partial_t m_o + \nabla\cdot\boldsymbol{F}_o = Q_o, \tag{12}$$
$$\text{Water:}\quad \partial_t m_w + \nabla\cdot\boldsymbol{F}_w = Q_w. \tag{13}$$

Denoting by S_w the water saturation,

$$m_o = \rho_o\phi(1-S_w), \tag{14}$$
$$m_w = \rho_w\phi S_w, \tag{15}$$

where ρ_o (resp. ρ_w) is the density of the oil (resp. water). The sources of each phase take the expressions:

$$Q_o = \rho_o\phi q_T(1-S_w^*), \tag{16}$$
$$Q_w = \rho_w\phi q_T S_w^*, \tag{17}$$

where S_w^* is the water saturation of the injected fluid. In the case of negative source ($q_T < 0$), the produced fluid has a water saturation equal to that of the reservoir ($S_w^* = S_w$).

Mass fluxes of each component are expressed in terms of the phase velocities $\boldsymbol{v}_o$ and $\boldsymbol{v}_w$:

$$\boldsymbol{F}_o = \rho_o\phi\boldsymbol{v}_o, \tag{18}$$
$$\boldsymbol{F}_w = \rho_w\phi\boldsymbol{v}_w. \tag{19}$$

The phase velocities are usually expressed through the multiphase extension of Darcy's law.[48] Excluding gravity, these take the form:

$$\boldsymbol{v}_o = -\frac{\mathbf{k}}{\phi}\frac{k_{ro}}{\mu_o}\nabla p_o, \tag{20}$$
$$\boldsymbol{v}_w = -\frac{\mathbf{k}}{\phi}\frac{k_{rw}}{\mu_w}\nabla p_w. \tag{21}$$

where k_{ro}, k_{rw} are the relative permeabilities, μ_o, μ_w are the dynamic viscosities, and p_o, p_w are the pressures of oil and water, respectively. We introduce, for convenience, the phase relative mobilities:

$$\lambda_o := \frac{k_{ro}}{\mu_o}, \quad \lambda_w := \frac{k_{rw}}{\mu_w}. \tag{22}$$

We express the phase pressures as:

$$p_o \equiv p, \tag{23}$$
$$p_w \equiv p - P_c, \tag{24}$$

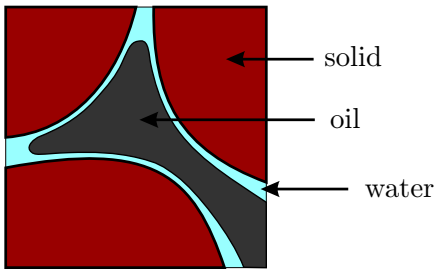

Figure 3: Schematic of immiscible flow of two fluid phases

where we choose the pressure variable p to be the oil-phase pressure, and P_c is the capillary pressure, assumed here to be a function of saturation. Defining the total velocity $\boldsymbol{v}_T := \boldsymbol{v}_w + \boldsymbol{v}_o$, the phase velocities take the form:

$$\boldsymbol{v}_o = \frac{\lambda_o}{\lambda_w + \lambda_o}\boldsymbol{v}_T - \frac{\lambda_w \lambda_o}{\lambda_w + \lambda_o}\frac{\mathbf{k}}{\phi}\nabla P_c, \tag{25}$$

$$\boldsymbol{v}_w = \frac{\lambda_w}{\lambda_w + \lambda_o}\boldsymbol{v}_T + \frac{\lambda_w \lambda_o}{\lambda_w + \lambda_o}\frac{\mathbf{k}}{\phi}\nabla P_c. \tag{26}$$

Assuming that the fluids and the medium are incompressible, addition of equations (12) and (13) yields the continuity (or "pressure") equation:

$$\nabla \cdot \boldsymbol{v}_T = q_T, \tag{27}$$

where the total velocity is obtained by adding the phase velocities (20)–(21), and using the phase pressures (23)–(24):

$$\boldsymbol{v}_T = -(\lambda_w + \lambda_o)\frac{\mathbf{k}}{\phi}\nabla p - \lambda_w \frac{\mathbf{k}}{\phi}\left(-\frac{\mathrm{d}P_c}{\mathrm{d}S_w}\right)\nabla S_w. \tag{28}$$

Substituting equations (15), (19) and (26) into (13), we get the "saturation" equation:

$$\partial_t S_w + \nabla \cdot \left[\boldsymbol{v}_T \frac{\lambda_w}{\lambda_w + \lambda_o} - \frac{\lambda_w \lambda_o}{\lambda_w + \lambda_o}\frac{\mathbf{k}}{\phi}\left(-\frac{\mathrm{d}P_c}{\mathrm{d}S_w}\right)\nabla S_w\right] = q_T S_w^* \tag{29}$$

We make the following observations:

1. As in the miscible case, the "pressure" equation is elliptic, and has to be solved for the pressure p and the total velocity $\boldsymbol{v}_T$.
2. The "saturation" equation is a conservation law of the advection-diffusion type, where the "diffusion" in the saturation equation is caused by capillarity, not by physical diffusion.
3. Both equations are nonlinear due to the nonlinearity of relative permeabilities and capillary pressure.
4. In contrast to the miscible case, equations (27) and (29) are coupled, because the total velocity depends on saturation. This coupling can be circumvented by defining a "global pressure".[1]

Numerical formulation: the multiscale approach

The need for an accurate velocity field has long been recognized, especially when the medium is highly heterogeneous. It has been shown[4,49–52] that mixed finite element methods (which discretize the pressure field and the velocity field simultaneously) are far superior to classical conforming methods (where velocities are obtained from differentiation of the pressure field) for the numerical solution of the "pressure" equation.

In any case, we focus on the solution of the "concentration" or "saturation" equation, and assume that the total velocity field is known. This is trivial for the 1D case, as $\boldsymbol{v}_T$ does not depend on position. The analogy between equations (11) and (29) allows us to present a unified treatment for miscible and immiscible flow in the framework of advection-diffusion conservation laws.

Initial and boundary value problem. The "concentration" equation (11) of miscible flow and the "saturation" equation (29) of immiscible flow are scalar conservation laws of the form:

$$\partial_t u + \nabla \cdot \boldsymbol{\mathcal{F}} = q, \quad x \in \Omega,\ t \in (0, T], \tag{30}$$

where u is the conserved quantity, $\boldsymbol{\mathcal{F}}$ is the total flux of that quantity, q is the rate of production (per unit volume), Ω is the spatial domain and $(0, T]$ is the time interval of interest. The total flux is of advection-diffusion type:

$$\boldsymbol{\mathcal{F}} = \boldsymbol{f}(u) - \mathbf{D}(u)\nabla u, \tag{31}$$

where $\boldsymbol{f}$ is the hyperbolic part of the flux and $\mathbf{D}$ is the diffusion tensor. Both are allowed to be nonlinear functions of the unknown u. In the linear case,

$$\boldsymbol{\mathcal{F}} = \boldsymbol{a}u - \mathbf{D}\nabla u, \tag{32}$$

where both $\boldsymbol{a}$ (the advective velocity) and $\mathbf{D}$ are independent of u. For this case we introduce the linear advection-diffusion operator in conservation form:

$$\mathcal{L}u := \nabla \cdot (\boldsymbol{a}u - \mathbf{D}\nabla u). \tag{33}$$

The equivalence between the generic variables introduced here and those of the previous section are given in **Table 1**.

Let $\partial\Omega$ be the boundary of the domain, $\Gamma_u \subset \partial\Omega$, $\Gamma_n = \partial\Omega \setminus \Gamma_u$, we shall consider the following boundary conditions (Dirichlet and Neumann, respectively):

$$u = \bar{u} \text{ on } \Gamma_u, \tag{34}$$

$$\boldsymbol{\mathcal{F}} \cdot \boldsymbol{n} = \bar{\mathcal{F}} \text{ on } \Gamma_n, \tag{35}$$

where $\boldsymbol{n}$ is the outward unit normal to the boundary. The initial conditions are

$$u(x, t = 0) = u_0(x). \tag{36}$$

Generic	Miscible flow	Immiscible flow
u	c	S_w
q	$q_T c^*$	$q_T S_w^*$
$\boldsymbol{f}$	$\boldsymbol{v}_T c$	$\boldsymbol{v}_T \dfrac{\lambda_w}{\lambda_w+\lambda_o}$
$\mathbf{D}$	$\mathbf{D}$	$\dfrac{\lambda_w\lambda_o}{\lambda_w+\lambda_o}\dfrac{\mathbf{k}}{\phi}\left(-\dfrac{\mathrm{d}P_c}{\mathrm{d}S_w}\right)$

Table 1: Equivalence of variables for the advection-diffusion conservation law

Weak form. Let us introduce the functional spaces:

$$\mathcal{V} := \{v \in W : v = \bar{u} \text{ on } \Gamma_u\},$$
$$\mathcal{V}_0 := \{v \in W : v = 0 \text{ on } \Gamma_u\},$$

where the appropriate choice of the Sobolev space W depends on the form of the diffusion tensor. The weak form of problem (30)–(31) with boundary and initial conditions (34)–(36) is to seek $u \in \mathcal{V}$ for each fixed $t \in (0,T]$, such that

$$\begin{aligned}(\partial_t u, v) + a(u, v; u) = l(v) \quad \forall v \in \mathcal{V}_0,\\ u(x, t=0) = u_0(x),\end{aligned} \tag{37}$$

where

$$(\partial_t u, v) = \int_\Omega \partial_t u\, v \,\mathrm{d}\Omega, \tag{38}$$

$$\begin{aligned}a(u, v; w) &= -\int_\Omega \boldsymbol{\mathcal{F}}(w, \nabla u)\cdot\nabla v \,\mathrm{d}\Omega\\ &= -\int_\Omega \boldsymbol{f}(w)\cdot\nabla v\,\mathrm{d}\Omega + \int_\Omega \mathbf{D}(w)\nabla u\cdot\nabla v\,\mathrm{d}\Omega,\end{aligned} \tag{39}$$

$$l(v) = \int_\Omega q v\,\mathrm{d}\Omega - \int_{\Gamma_n} \bar{\mathcal{F}} v\,\mathrm{d}\Gamma. \tag{40}$$

The weak form of the *linear* problem is to find $u \in \mathcal{V}$ for each fixed $t \in (0,T]$, such that

$$\begin{aligned}(\partial_t u, v) + a(u, v) = l(v) \quad \forall v \in \mathcal{V}_0,\\ u(x, t=0) = u_0(x).\end{aligned} \tag{41}$$

The only difference with respect to Equation (37) is that $a(u,v) \equiv a(u,v;u)$ is now a *bilinear* form.

Classical Galerkin method. Let $\mathcal{V}_h \subset \mathcal{V}$, and $\mathcal{V}_{h,0} \subset \mathcal{V}_0$, be *conforming* finite element spaces of piecewise polynomials. The standard Galerkin approximation of (37) is simply to find $u_h \in \mathcal{V}_h$ for each fixed t, such that

$$(\partial_t u_h, v_h) + a(u_h, v_h; u_h) = l(v_h) \quad \forall v_h \in \mathcal{V}_{h,0}, \tag{42}$$

and $u_h(x, t=0)$ is the projection of the initial function $u_0(x)$ onto space $\mathcal{V}_h$. This constitutes a system of nonlinear ordinary differential equations. The fully discrete system is obtained by further discretizing in time. It is well known that the standard Galerkin method lacks stability for the near-hyperbolic problem (in the numerical simulations we shall see examples of this behavior).

Multiscale approach for the linear advection-diffusion equation. The *key idea* of the proposed methodology is to consider the continuous spaces $\mathcal{V}$ and $\mathcal{V}_0$ as the direct sum of two spaces,

$$\mathcal{V} = \mathcal{V}_h \oplus \tilde{\mathcal{V}}, \qquad \mathcal{V}_0 = \mathcal{V}_{h,0} \oplus \tilde{\mathcal{V}}, \tag{43}$$

where $\mathcal{V}_h$ and $\mathcal{V}_{h,0}$ are the spaces of *resolved scales* and $\tilde{\mathcal{V}}$ is the space of *subgrid scales*. This decomposition was first proposed by Hughes,[43] and it acknowledges the fact that the fine scale of the solution cannot be captured by the finite element mesh. However, the influence of the subscales on the grid scales is *not* negligible. We can now split problem (41) into two, one for the *grid scales*,

$$(\partial_t(u_h+\tilde{u}), v_h) + a(u_h+\tilde{u}, v_h) = l(v_h) \quad \forall v_h \in \mathcal{V}_{h,0}, \tag{44}$$

and one for the *subscales*,

$$(\partial_t(u_h+\tilde{u}), \tilde{v}) + a(u_h+\tilde{u}, \tilde{v}) = l(\tilde{v}) \quad \forall \tilde{v} \in \tilde{\mathcal{V}}. \tag{45}$$

We now assume the subscales are quasistatic,[53] i.e., $\partial_t \tilde{u} \approx 0$. Integrating by parts on each element and making use of the linearity of $a(\cdot,\cdot)$ and continuity of diffusive fluxes of $u = u_h + \tilde{u}$ across interelement boundaries,[54] we get the following equation for the subscales:

$$\sum_e \int_{\Omega^e} \tilde{v}\,\mathcal{L}\tilde{u}\,\mathrm{d}\Omega = \sum_e \int_{\Omega^e} \tilde{v}\,(q - \partial_t u_h - \mathcal{L}u_h)\,\mathrm{d}\Omega \quad \forall \tilde{v} \in \tilde{\mathcal{V}}. \tag{46}$$

Defining the *grid scale residual* $\mathcal{R}u_h := q - \partial_t u_h - \mathcal{L}u_h$, we can understand Equation (46) in a strong sense,

$$\tilde{\Pi}(\mathcal{L}\tilde{u}) = \tilde{\Pi}(\mathcal{R}u_h), \tag{47}$$

where $\tilde{\Pi}$ is the L^2-projection onto the space of subgrid scales. Rather than solving this problem, we *model* it using an algebraic subgrid scale (ASGS) approximation:[54]

$$\tilde{u} \approx \tau \mathcal{R}u_h. \tag{48}$$

The algebraic operator τ is called the *relaxation time*. Its design, usually dictated by convergence analysis, has profound implications from a physical and numerical viewpoint. Here we use the following expression:[54]

$$\tau = \left(c_1 \frac{\|\mathbf{D}\|}{h^2} + c_2 \frac{|\boldsymbol{a}|}{h}\right)^{-1}, \tag{49}$$

where h is a characteristic length of the element under consideration, and $c_1 = 4$, $c_2 = 2$ for linear elements.[45,54] This completes the description of the subgrid scales.

After integration by parts on each element of the term $a(\tilde{u}, v_h)$ in Equation (44), the equation for the grid scales reads

$$(\partial_t u_h, v_h) + a(u_h, v_h) + \sum_e \left[\int_{\Omega^e} \tilde{u}\, \mathcal{L}^* v_h \, \mathrm{d}\Omega + \int_{\Gamma^e} \tilde{u}\, b^* v_h \, \mathrm{d}\Gamma \right] = l(v_h) \quad \forall v_h \in \mathcal{V}_{h,0}, \quad (50)$$

where $\mathcal{L}^* v := -\boldsymbol{a} \cdot \nabla v - \nabla \cdot (\mathbf{D} \nabla v)$ is the adjoint of $\mathcal{L}$, and $b^* v := (\mathbf{D} \nabla v) \cdot \boldsymbol{n}$ is the associated boundary operator. It is important to note the following:

1. The final equation for the resolved scales, Equation (50), includes the usual Galerkin terms (see Equation (42)) and some additional volume and boundary integrals evaluated element by element. These stabilizing terms, which are similar to those of other stabilized formulations,[45] arise naturally in the multiscale approach.[43,44]
2. The contribution from the boundary integrals in (50) has been neglected in the calculations. This is sensible only when the process is *not* dominated by diffusion.
3. The subscales $\tilde{u}$ are modeled analytically and eliminated from the global problem. With the algebraic approximation used here, they are proportional to the grid scale residual (see Equation (48)). The method is residual-based and, therefore, automatically consistent.

Multiscale approach for the nonlinear advection-diffusion equation. This section deals with the nonlinear problem given by Equations (30)–(36). Extension of the multiscale approach to nonlinear problems is not straightforward, mainly because the form $a(u, v; w)$ in Equation (37) is not linear in w. Linearizing the equations upfront is not desirable when the solution is nonsmooth, since the conservation properties of the method might be compromised.[55] Our approach is based on an incremental formulation and a multiple scale decomposition of the increment,

$$u^{(k+1)} \approx u_h^{(k)} + \delta u^{(k)} = u_h^{(k)} + \delta u_h^{(k)} + \delta \tilde{u}^{(k)}, \quad (51)$$

where the index (k) refers to the iteration level. In this context, the incremental subscale $\delta \tilde{u}^{(k)}$ may be understood as a perturbation, i.e.,

$$u^{(k+1)} \approx u_h^{(k+1)} + \delta \tilde{u}^{(k)}. \quad (52)$$

In what follows, we shall omit superscripts referring to the iteration level and simply write: $u \approx u_h + \delta \tilde{u}$. Since the form $a(u, v; w)$ is linear with respect to the second argument (test function), the multiscale approach for problem (37) leads to a grid scale problem:

$$(\partial_t (u_h + \delta \tilde{u}), v_h) + a(u_h + \delta \tilde{u}, v_h; u_h + \delta \tilde{u}) = l(v_h) \quad \forall v_h \in \mathcal{V}_{h,0}, \quad (53)$$

and a subscale problem:

$$(\partial_t (u_h + \delta \tilde{u}), \tilde{v}) + a(u_h + \delta \tilde{u}, \tilde{v}; u_h + \delta \tilde{u}) = l(\tilde{v}) \quad \forall \tilde{v} \in \tilde{\mathcal{V}}. \quad (54)$$

Expanding the constitutive relations $\boldsymbol{f}(u)$ and $\mathbf{D}(u)$ to first order about an approximate coarse-scale solution u_h, integrating by parts on each element some of the terms, assuming continuous interelement fluxes for the solution u, and considering quasistatic subscales as before, Equation (54) takes the form

$$\sum_e \int_{\Omega^e} \tilde{v}\, \nabla \cdot \left[(\boldsymbol{f}'(u_h) - \mathbf{D}'(u_h) \nabla u_h) \delta \tilde{u} - \mathbf{D}(u_h) \nabla \delta \tilde{u} \right] \mathrm{d}\Omega = \sum_e \int_{\Omega^e} \tilde{v}\, \left[q - \partial_t u_h - \nabla \cdot (\boldsymbol{f}(u_h) - \mathbf{D}(u_h) \nabla u_h) \right] \mathrm{d}\Omega. \quad (55)$$

The variable $\boldsymbol{a}(u_h) := \boldsymbol{f}'(u_h) - \mathbf{D}'(u_h) \nabla u_h$ plays the role of an advective velocity. Defining the *linearized operator* $\mathcal{L}_{u_h} v := \nabla \cdot [\boldsymbol{a}(u_h) v - \mathbf{D}(u_h) \nabla v]$, the expression above is written succinctly as

$$\sum_e \int_{\Omega^e} \tilde{v}\, \mathcal{L}_{u_h} \delta \tilde{u} \, \mathrm{d}\Omega = \sum_e \int_{\Omega^e} \tilde{v}\, \mathcal{R}(u_h) \, \mathrm{d}\Omega \quad \forall \tilde{v} \in \tilde{\mathcal{V}}. \quad (56)$$

Using an algebraic approximation to the subscales, the equation for the subgrid scales is, finally,

$$\delta \tilde{u} \approx \tau_{u_h} \mathcal{R}(u_h), \quad (57)$$

where τ_{u_h} is now a nonlinear function of the grid scale solution u_h. Integrating by parts some of the terms in Equation (53) and rearranging conveniently, the coarse-scale equation reads

$$(\partial_t u_h, v_h) + a(u_h, v_h; u_h) + \sum_e \left[\int_{\Omega^e} \delta \tilde{u}\, \mathcal{L}^*_{u_h} v_h \, \mathrm{d}\Omega + \int_{\Gamma^e} \delta \tilde{u}\, b^*_{u_h} v_h \, \mathrm{d}\Gamma \right] = l(v_h) \quad \forall v_h \in \mathcal{V}_{h,0}, \quad (58)$$

where $\mathcal{L}^*_{u_h} v := -\boldsymbol{a}(u_h) \cdot \nabla v - \nabla \cdot (\mathbf{D}(u_h) \nabla v)$ is the adjoint of the *linearized* operator $\mathcal{L}_{u_h}$, and $b^*_{u_h} v := (\mathbf{D}(u_h) \nabla v) \cdot \boldsymbol{n}$ is the associated boundary operator. Equations (57) and (58) define the algebraic subgrid scale finite element method for a nonlinear advection-diffusion equation. Let us make the following remarks:

1. Equations (57) and (58) are analogous to equations (48) and (50) for the linear case. In both cases, the formulation is residual-based and, thus, automatically consistent. In the nonlinear case, both coarse-scale and subgrid-scale equations need to be solved using an iterative procedure, e.g., Newton's method.
2. Application of the multiple scale framework to nonlinear problems was investigated for one-dimensional strain localization.[56] In this reference, the incremental solution $\delta u = \delta u_h + \delta \tilde{u}$ was reconstructed after each iteration.

We further improve the method by incorporating a *shock-capturing* technique, based on increasing the amount of numerical dissipation in the neighborhood of layers.[10] By doing this, we avoid oscillations where sharp features occur, while keeping the method high-order accurate in smooth regions. The discontinuity-capturing scheme consists in adding the following integral to the left-hand side of Equation (58):

$$\sum_e \int_{\Omega^e} D_{sc}(u_h) \nabla u_h \cdot \nabla v_h \, d\Omega, \tag{59}$$

where D_{sc} is a nonlinear diffusion coefficient. This leads necessarily to a nonlinear method, even if the underlying equation is linear. The success of this technique depends on the design of the numerical diffusion. The "canonical" form of the artificial diffusion is:[10]

$$D_{sc} = \alpha_{sc} h \frac{|\mathcal{R}(u_h)|}{|\nabla u_h|} \tag{60}$$

where

$$\alpha_{sc} = \max\left(0, C_{sc} - \frac{1}{P_e}\right), \tag{61}$$

P_e being the element Peclet number and C_{sc} a constant coefficient. In the advective limit, α_{sc} approaches a constant value and, for steady-state conditions and linear elements, $\mathcal{R}(u_h) = -\boldsymbol{a} \cdot \nabla u_h$. For one-dimensional problems this gives the same artificial diffusion everywhere, even though numerical dissipation is required *only* in the vicinity of sharp gradients. In this investigation, we propose a novel dimensionally-consistent, *subscale-driven* artificial diffusion, given by

$$D_{sc} = C_{sc} \frac{|\delta \tilde{u}|}{U_{sc}} h |\boldsymbol{a}(u_h)|, \tag{62}$$

where U_{sc} is a characteristic value of the solution near the shock, and C_{sc} is a constant coefficient. The added numerical diffusion will be significant only where the absolute value of the subgrid scales *and* the advective velocity are important.

Representative numerical simulations

In this section we present some numerical simulations of miscible and immiscible flow. All test cases are initially transient, but eventually reach stationary (or quasi-stationary) conditions. We compare the results obtained with the proposed multiscale formulation with those of Galerkin method, to illustrate the enhanced stability properties of the former. For some test cases, we also show the effect of shock-capturing on the numerical solution, and we compare the performance of the "canonical" form and the subscale-driven form of the discontinuity-capturing dissipation. Convergence behavior of Newton iteration is also discussed.

One-dimensional miscible flow. For one-dimensional problems, the flux vector and the diffusion tensor in Equation (31) reduce to scalar quantities. In miscible flow, the hyperbolic part of the flux function is $f(u) = au$, where $a = v_T$ is the fluid velocity. A common formulation of the diffusion coefficient is:[48]

$$D = D_m + \alpha_L v_T, \tag{63}$$

where D_m is the molecular diffusion coefficient, and α_L is the longitudinal dispersivity. The net effect of hydrodynamic dispersion is an additional diffusion, which would smear out the fronts and reduce considerably the complexity of the problem. Therefore, we take $\alpha_L = 0$ and use $D = \epsilon = \text{const}$. The final equation to be solved is the scalar linear advection-diffusion equation in 1D:

$$\partial_t u + \partial_x (au - \epsilon \partial_x u) = q. \tag{64}$$

Test Case 1: zero distributed sources. We solve the problem on a unit segment $\Omega = [0, 1]$ with Dirichlet boundary conditions $u(0, t) = 1$, $u(1, t) = 0$, zero initial data and no distributed sources. The advection velocity is $a = 1$ and the constant diffusion coefficient is $\epsilon = 10^{-4}$, which makes the problem almost hyperbolic. Solution obtained by Galerkin method and the subgrid scale approach (ASGS), with and without shock-capturing, are compared against the analytical solution for a very coarse ($N_e = 20$, $\delta t = 0.01$) and a finer ($N_e = 100$, $\delta t = 0.002$) discretization. Linear elements and a Crank-Nicolson time-stepping scheme were used in all cases. It is worth noting that the element Peclet number is as high as 500 for the coarse grid, and 100 for the "fine" grid.

The solution displays a moving front during the transient phase, and develops a very sharp boundary layer when stationary conditions are reached. All methods predict the speed of the front accurately, even with the coarse mesh. The ASGS method is able to reduce the oscillations near the front compared with Galerkin method, as shown in **Figures 4(a)** (coarse mesh) and **4(b)** (fine mesh) for observation times $t = 0.2$ and $t = 0.5$. However, the most relevant difference arises for long simulation times, when the solution is steady state (shown for $t = 2.0$). Classical Galerkin solution shows spurious oscillations in the entire domain, whereas the ASGS solution has no oscillations whatsoever and is extremely accurate: the boundary layer is captured within a single element.

Localized wiggles of the ASGS solution during transient conditions are further reduced by using a shock-capturing technique, as described in the previous section. Two different formulations are used for the discontinuity-capturing numerical dissipation: the "canonical" form (CASC) given by Equation (60), and the subscale-driven form (SGSC) of Equation (62). In **Figure 4(c)** we plot the profile of numerical diffusion added by each of these formulations for the coarse grid at two different times: $t = 0.5$ (transient conditions) and $t = 2.0$ (stationary conditions). The "canonical" form of shock-capturing diffusion displays an erratic oscillatory behavior for transient conditions, with

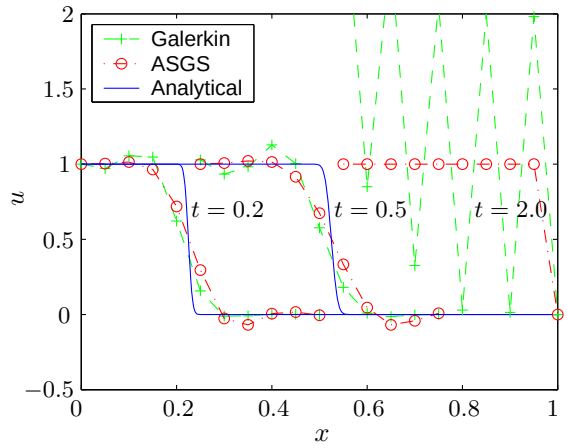

(a) Coarse grid. Galerkin vs. ASGS

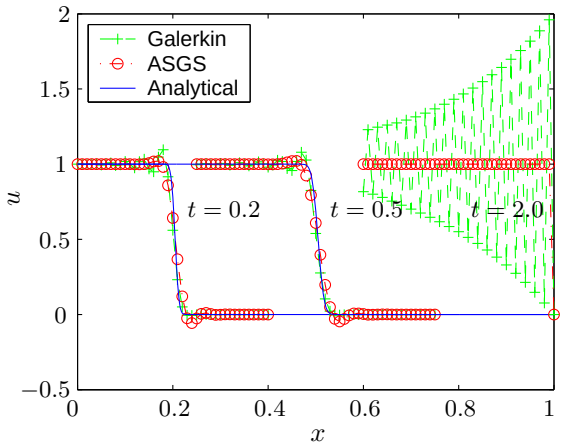

(b) Fine grid. Galerkin vs. ASGS

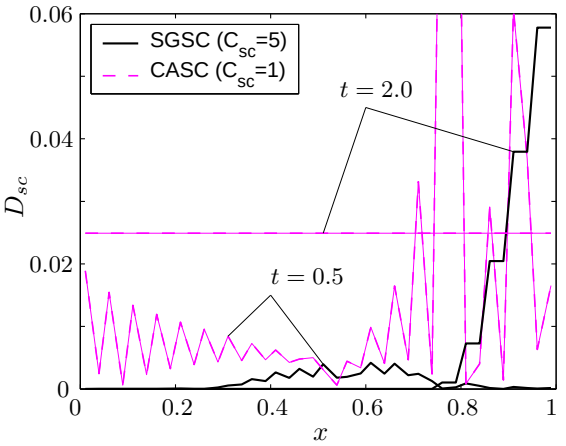

(c) Coarse grid. Shock-capturing diffusion

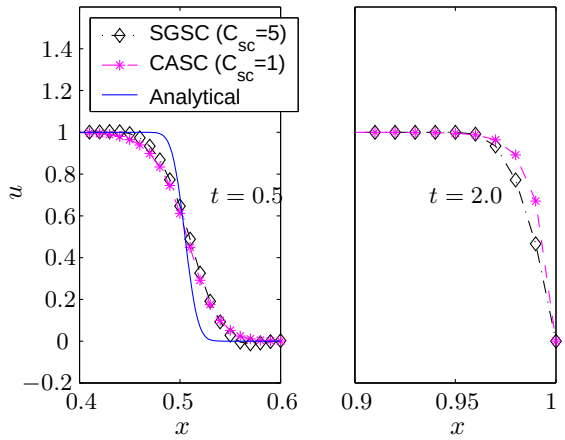

(d) Fine grid. ASGS with shock-capt

Figure 4: 1D miscible flow with zero distributed sources. ASGS vs. Galerkin solution and ASGS with shock-capturing at three different times, for a very coarse (left) and a finer (right) discretization

significant diffusion everywhere and not just in the vicinity of the front. When steady state is met, the artificial diffusion added by this model is constant over the entire domain, which is in disagreement with the very concept of discontinuity capturing. On the other hand, the novel formulation of nonlinear dissipation proportional to the absolute value of the subscales gives the expected behavior: the profile of artificial diffusion has a maximum value near the location of the layer, and decays rapidly away from it. A detail of the numerical solutions obtained by the ASGS method with shock-capturing are shown in **Figure 4(d)** for the fine grid. Both discontinuity-capturing schemes are effective at reducing localized oscillations near the layers.

When the shock-capturing technique is used, the method is nonlinear even if the underlying equation is linear, because the the amount of dissipation is a nonlinear function of the solution. A Newton iterative scheme was used to achieve convergence at every time step. In **Figure 5** we show the evolution of the L_2-norm of the residual for a typical time step (in this case $t = 0.5$). The ASGS method with subscale-driven shock-capturing converges quadratically for all time steps. Convergence when the "canonical" form of discontinuity-capturing is used is always slower and often not monotonic. This is not surprising given the erratic behavior of the numerical diffusion introduced by the method (**Figure 4(c)**).

Test Case 2: nonzero distributed sources. This test case was developed to investigate the effect of distributed source terms on the proposed stabilized finite element method. The equation to be solved and all the parameters are identical to those of Test Case 1, except for homogeneous Dirichlet boundary conditions and a constant distributed source $q = 1$. Solution by Galerkin method and the subgrid scale method at three different times are shown in **Figure 6**. Both have been computed using a backward Euler time-stepping scheme and a rela-

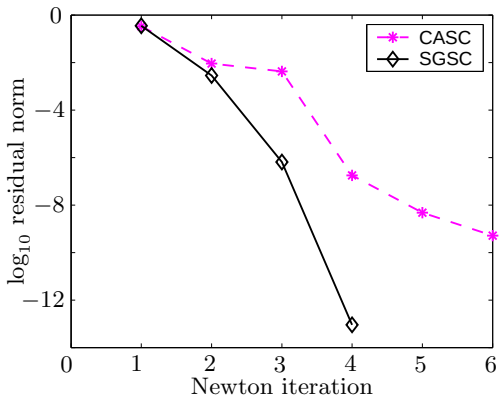

Figure 5: 1D miscible flow with zero distributed sources. Convergence of the ASGS method with shock-capturing at $t = 0.5$

tively coarse grid: $N_e = 40$, $\delta t = 0.01$. The corresponding element Peclet number is 250.

During the transient phase, the concentration profile consists of a rising plateau due to the source term, and a ramp of slope q/a due to the advection term. A boundary layer forms at the right end even for early times, in order to satisfy the Dirichlet boundary condition. Under this situation, classical Galerkin method produces a globally oscillatory solution at all times. On the other hand, the solution obtained by the ASGS method is nonoscillatory. Still, it captures sharply the transition at the moving ramp-plateau interface, and the boundary layer with a single element.

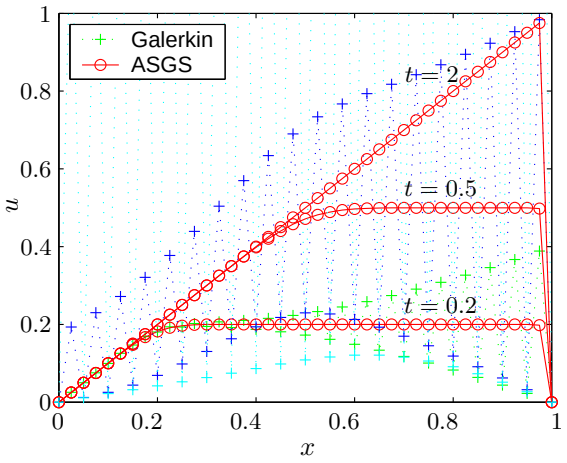

Figure 6: 1D miscible flow with nonzero distributed sources. ASGS vs. Galerkin solution at three different times

Two-dimensional miscible flow. We follow the same arguments as in the one-dimensional case, i.e.,

1. We assume the velocity field from the "pressure" equation, $\boldsymbol{a} = \boldsymbol{v}_T$, is known.

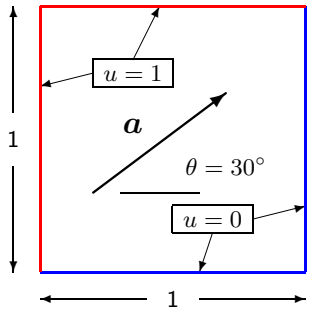

Figure 7: Schematic of the 2D miscible flow problem

2. We neglect the effects of hydrodynamic dispersion, so that $\mathbf{D} = \epsilon \mathbf{I}$, where $\mathbf{I}$ is the 2×2 identity tensor.

The equation governing the transport of the tracer is the scalar linear advection-diffusion equation in 2D:

$$\partial_t u + \nabla \cdot (\boldsymbol{a} u - \epsilon \nabla u) = q. \tag{65}$$

We solve this equation on the unit square $\Omega = [0,1] \times [0,1]$, with homogeneous Dirichlet boundary conditions on the bottom and right edges ($u = 0$ on $x = 1, y = 0$), and unit Dirichlet boundary conditions on the top and left edges ($u = 1$ on $x = 0, y = 1$). We take a uniform velocity field of unit magnitude, tilted 30° with respect to the x-axis, $\boldsymbol{a} = (\cos 30°, \sin 30°)$, so that it is not aligned with the mesh. We consider a very small diffusion coefficient $\epsilon = 10^{-6}$, and no distributed sources ($q = 0$). A schematic of this test case is shown in **Figure 7**.

During the transient phase, the solution displays a front moving from left to right, an internal layer forming a 30°-angle with the bottom boundary, and a boundary layer at the top edge. Once the moving front reaches the right boundary, stationary conditions are established. The sharp features of the steady-state solution include an internal layer, which develops from the lower-left corner and is tilted 30°, and a boundary layer at the upper part of the right boundary, required to satisfy the homogeneous boundary condition at the right edge.

We solve the problem using a uniform grid of 20×20 bilinear quadrilaterals, and backward Euler time-stepping with $\delta t = 0.01$. The element Peclet number is 50,000. Such coarse mesh is clearly insufficient to resolve the abrupt discontinuities of the solution, but the objective is to analyze the stability properties of the numerical method, i.e., whether the inaccuracies will propagate to produce a globally oscillatory solution.

Solution obtained by Galerkin method is completely oscillatory both for transient and stationary conditions (**Figures 8(a)** and **8(c)**). This behavior is in agreement with the well-known lack of stability of Galerkin method for advection-dominated problems. In contrast, the subgrid-scale formulation (ASGS method) produces an effectively stabilized solution. It captures rather sharply the advancing front during the transient phase and the internal and boundary layers which develop at steady state

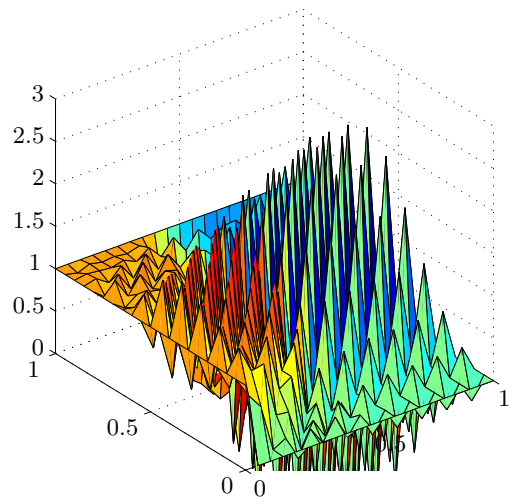

(a) Galerkin solution, $t = 0.5$

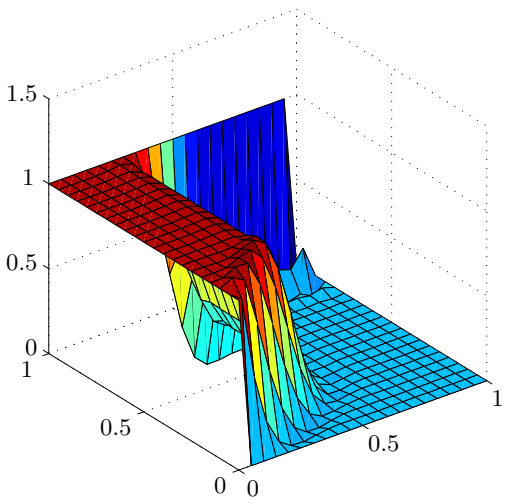

(b) ASGS solution, $t = 0.5$

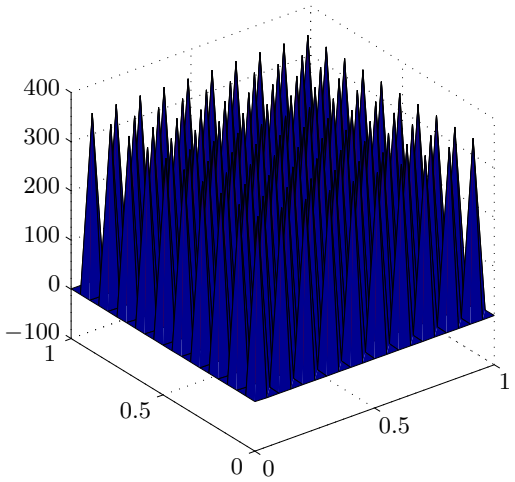

(c) Galerkin solution, steady-state

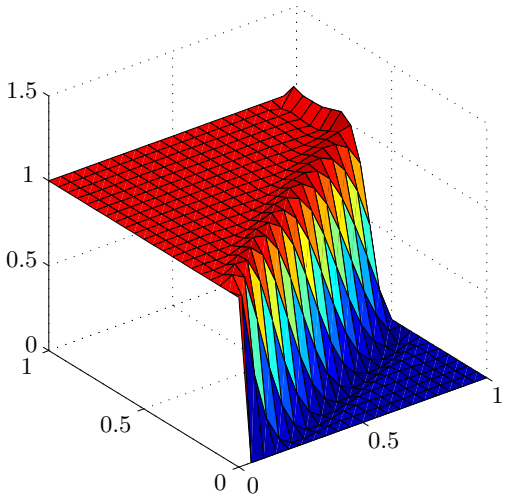

(d) ASGS solution, steady-state

Figure 8: 2D miscible flow. Galerkin and ASGS solutions for transient and steady-state conditions

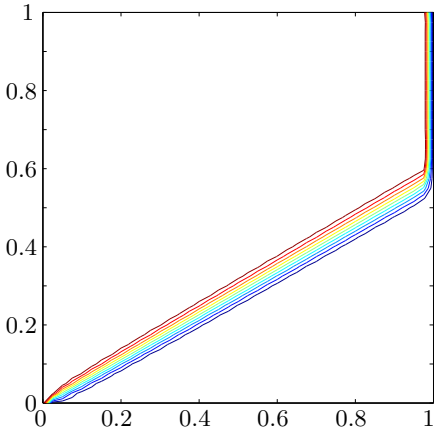

(a) ASGS solution, 40×40 elmts.

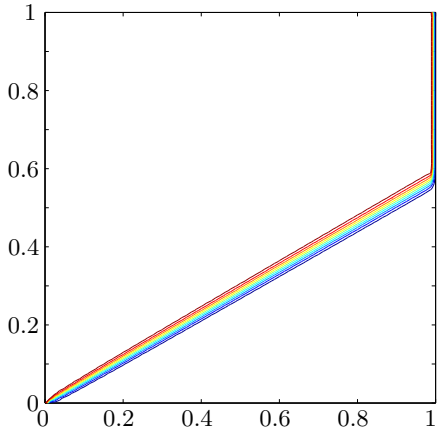

(b) ASGS solution, 80×80 elmts.

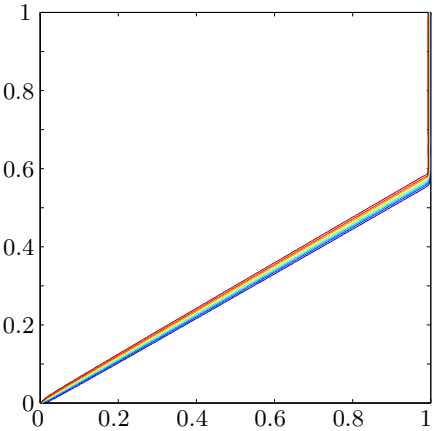

(c) ASGS solution, 125×125 elmts.

Figure 9: 2D miscible flow. Contour plots at steady-state on a 40×40, 80×80 and 125×125 grid

(**Figures 8(b)** and **8(d)**). It is important to note that the ASGS method only requires computation of some additional integrals, evaluated element-by-element, so the computational cost is roughly the same as that of Galerkin method. Local overshoots in the vicinity of discontinuities, which are still present in the stabilized solution, could be further reduced or completely removed using a shock-capturing technique,[10] as in the one-dimensional case. This possibility was not explored here.

In **Figure 9**, we show contour plots of the ASGS solution at steady state (contours correspond to the values $u = 0.1, 0.2, \ldots, 0.9$) for increasingly refined grids. This shows the type of convergence of the ASGS solution as the mesh is refined.

One-dimensional immiscible flow. Flow of two incompressible immiscible fluids, ignoring gravitational effects, is described by equations (30)–(31), where all variables are defined in Table 1. For the one-dimensional case, all vectors and tensors reduce to scalar quantities, and the equation is known as Buckley-Leverett equation.[57] The hyperbolic part of the flux function (fractional flow) is typically S-shaped and, thus, nonconvex. Assuming power-law expressions for the relative permeabilities,[37,55] the fractional flow function takes the form:

$$f(u) = v_T \frac{u^p}{u^p + r(1-u)^p}, \tag{66}$$

where p is the exponent of the power law, and $r := \mu_w/\mu_o$ is the viscosity ratio. The diffusion coefficient is degenerate for $u = 0$ and $u = 1$, and positive otherwise.[1] To mimic this behavior, we choose the following expression:[37]

$$D(u) = \epsilon u(1-u). \tag{67}$$

We solve the Buckley-Leverett equation on a unit segment $\Omega = [0,1]$ with Dirichlet boundary conditions $u(0,t) = 1$, $u(1,t) = 0$, and zero initial conditions. The total velocity is $v_T = 1$ and the constant in the degenerate diffusion coefficient is $\epsilon = 10^{-4}$. We take $p = 2$ and $r = 1$ in the expression for the fractional flow. When capillarity is neglected, the diffusion-free hyperbolic problem admits a self-similar solution, which consists of a rarefaction wave and a shock. Both the shock speed and the post-shock value are constant, and easily computable from the flux function.[55] Dirichlet boundary conditions are particularly challenging, because they force a very fast initial transient at the inlet, and a sharp boundary layer at the outlet after breakthrough. This problem "exhibits several difficult features beyond the usual ones of advection-dominated flow: degenerate diffusion, sharpening near-shock solutions, and capillary outflow boundary layers".[37] Numerical solutions to the Buckley-Leverett problem include the early works of Todd et al.,[58] Aziz and Settari[46,59] and, more recently, Dahle et al.,[37] and Binning and Celia.[60] The following numerical methods were tested in this investigation:

1. Galerkin: standard Galerkin approximation (Equation (42)).
2. ASGS: multiscale formulation, with an algebraic approximation to the subgrid-scales (Equation (58)).
3. CASC: ASGS method with "canonical" shock-capturing dissipation (Equation (60)).
4. SGSC: ASGS method with "subgrid-scale" shock-capturing dissipation (Equation (62)).

Results for a very coarse grid ($N_e = 20$, $\delta t = 0.01$) and a fine grid ($N_e = 500$, $\delta t = 0.0005$) are provided, which correspond to element Peclet numbers of $P_e \approx 2,500$ and $P_e \approx 100$, respectively.* In all cases we used a backward Euler time-stepping scheme.

In **Figure 10(a)** we plot the numerical solutions obtained by the standard Galerkin method and the ASGS method on the coarse grid, together with the analytical solution of the hyperbolic problem. Both numerical solutions predict correctly the shock location.† Classical Galerkin method produces a big overshoot upstream of the front during the transient state and, more noticeably, a completely oscillatory solution as the system approaches steady-state. On the other hand, the numerical solution obtained by the ASGS method is not globally polluted with oscillations, is very accurate where the analytical solution is smooth (outside a thin layer containing the discontinuities), and preserves a sharp definition of the saturation front and the boundary layer. However, small localized wiggles remain at the downstream end of the front for transient conditions, and one single major overshoot is present for the long-time solution. These observations are further confirmed by the numerical solution on the fine grid (**Figure 10(b)**). Only the ASGS solution is shown for the fine grid, as Galerkin method diverged before reaching the observation time $t = 1$.

We analyze the effect of using a shock-capturing scheme in conjunction with the ASGS method, and compare the performance of the "canonical" form (CASC) and the "subgrid-scale" form (SGSC). In **Figure 10(c)** we plot the profiles of artificial diffusion added by each method on the coarse grid at two different times. For both methods, the amount of numerical dissipation is significant only in the neighborhood of layers, but it decays more rapidly for the SGSC formulation. In **Figure 10(d)** we show magnified plots of all three numerical solutions (ASGS, CASC and SGSC) computed on the fine grid at times $t = 0.4$ and $t = 1$. Both shock-capturing schemes are effective at reducing or eliminating local overshooting, the novel SGSC formulation being (slightly) less diffusive.

*This should be compared with the simulations using characteristics methods,[37,60] where the highest Peclet number considered is about 2.

†Correct prediction of the shock location and convergence to the physically correct solution for the Galerkin method is in contrast to the findings of Todd et al.[58] and Aziz and Settari,[46] where midpoint weighting (equivalent to classical Galerkin) is shown to converge to a nonphysical solution. The reason for this discrepancy[55] is that the conservation form of the "saturation" equation is used here, whereas the aforementioned references discretize a nonconservation form.

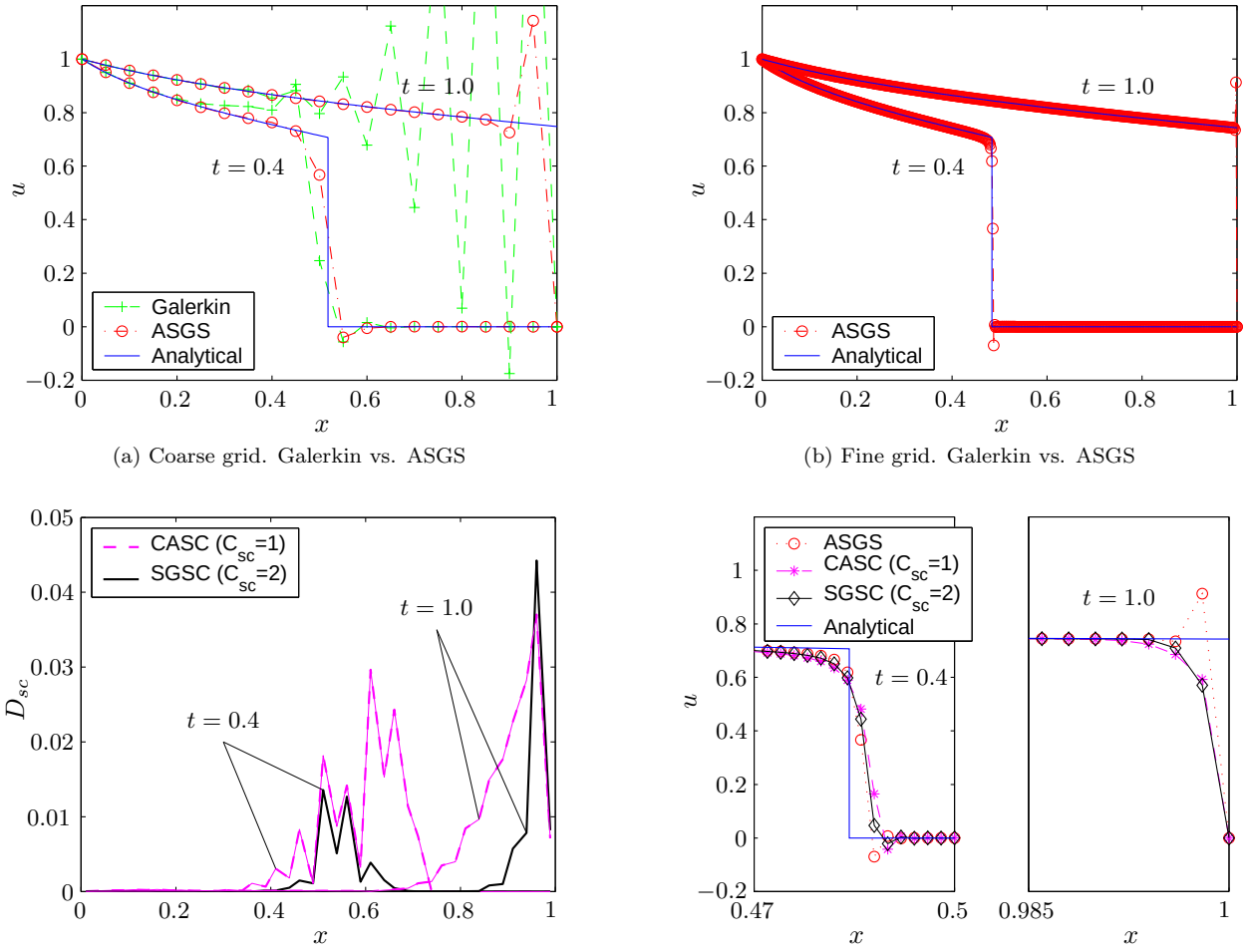

(a) Coarse grid. Galerkin vs. ASGS

(b) Fine grid. Galerkin vs. ASGS

(c) Coarse grid. Shock-capturing diffusion

(d) Fine grid. ASGS with shock-capturing

Figure 10: 1D immiscible flow. ASGS vs. Galerkin solution and ASGS with shock-capturing at two different times, for a very coarse (left) and a fine (right) discretization

A Newton scheme was used in all cases to solve the system of nonlinear algebraic equations at each time step. In **Figure 11** we show the evolution of the L_2-norm of the residual for two typical time steps (shown are $t = 0.4$ and $t = 1$) of the coarse grid simulations. The main observation is that convergence is monotonic and asymptotically quadratic for all methods. The CASC and SGSC methods (with shock-capturing diffusion) take one or two more iterations during the transient period, while the situation is reversed for steady state.

Conclusions

We have presented a successful numerical method for the solution of nonlinear conservation laws, which is based on a multiscale decomposition of the variables of interest, and applied it to problems of miscible and immiscible two-phase flow in porous media. To the best of our knowledge, this approach is entirely new in the context of flow in porous media and reservoir simulation. The key idea is to acknowledge that the fine-scale structure of the solution cannot be captured by any grid, and to incorporate the net effect of the subgrid scales into the scales resolved by the mesh. The multiscale approach leads to stabilized finite element methods, which are not overly diffusive. The method does not emanate from a monotonicity argument, and the numerical solution may exhibit localized wiggles near discontinuities. To further reduce or completely eliminate these local oscillations, we have presented a novel subscale-driven shock-capturing scheme, based on adding a nonlinear dissipation proportional to the absolute value of the subscales. In the test cases studied, the new formulation of discontinuity-capturing yields better performance than "canonical" formulations.

Several issues regarding the numerical formulation deserve further investigation:

1. The effect of neglecting the contribution from the interelement boundary integrals to the stabilizing term.[44]

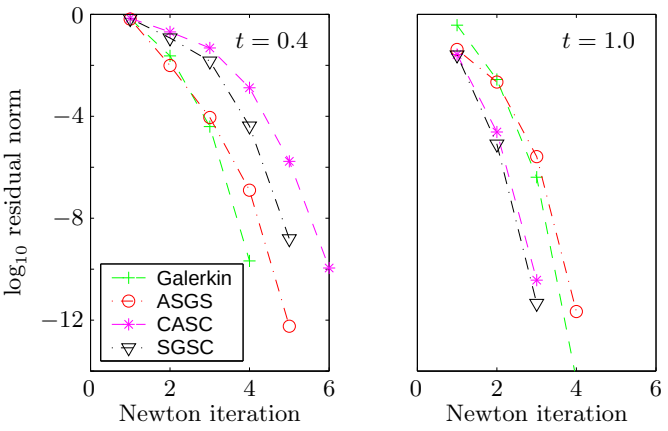

Figure 11: 1D immiscible flow. Convergence of the Newton iterative scheme for two typical time steps

2. Consistency of low-order implementations, where the high-order derivatives of the grid-scale residual are not captured by the finite element interpolation.[61]

3. Tracking of subscales in time for transient problems.[53,62]

4. Reconstruction of the solution (grid and subgrid) at each time step.[56]

5. Modeling of subgrid scales: in this paper, an analytical algebraic approximation to the subscales (ASGS) was used. However, many other options are possible, including bubble functions,[63,64] wavelets,[65] subgrid diffusion[66,67] and multilevel methods.[68,69]

Of particular interest would be to investigate how the approximation of the subscales behaves as a physical model. In fact, the multiscale approach presented here provides a framework to incorporate the effect of the microscales on the macroscales, even if these two separate scales are governed by different fundamental processes.

We are now extending this methodology to multiphase compositional flows in multidimensions. Future work will deal with two-phase flow in 2D and 3D, three-phase immiscible flow in one space dimension (for which an analytical solution can be developed), and black-oil and compositional models in several dimensions.

Nomenclature

Roman letters

$a(\cdot,\cdot,\cdot)$ = form in the weak formulation
$\boldsymbol{a}$ = advective velocity, L/t
b^* = boundary operator associated with $\mathcal{L}^*$, L/t
$b^*_{u_h}$ = boundary operator associated with $\mathcal{L}^*_{u_h}$, L/t
c = mass fraction of tracer, dimensionless
c^* = tracer mass fraction of the source, dimensionless
c_1, c_2 = constants in the definition of τ, dimensionless
C_{sc} = constant in the shock-capturing diffusion, dimensionless
$\mathbf{D}$ = diffusion tensor, L^2/t
D_m = molecular diffusion coefficient, L^2/t
D_{sc} = shock-capturing diffusion, L^2/t
$\boldsymbol{f}$ = hyperbolic part of the flux $\boldsymbol{\mathcal{F}}$, L/t
$\boldsymbol{\mathcal{F}}$ = total flux of u, L/t
$\bar{\mathcal{F}}$ = outward flux for Neumann boundary conditions, L/t
$\boldsymbol{F}_i$ = mass flux of species i, $\mathrm{m/L^2t}$
$\boldsymbol{F}_T$ = total fluid mass flux, $\mathrm{m/L^2t}$
h = characteristic length of an element, L
$\mathbf{k}$ = absolute permeability tensor, L^2
$k_{r\alpha}$ = relative permeability of the α-phase, dimensionless
$\mathcal{L}$ = linear advection-diffusion operator, 1/t
$\mathcal{L}^*$ = adjoint of $\mathcal{L}$, 1/t
$\mathcal{L}_{u_h}$ = linearized advection-diffusion operator, 1/t
$\mathcal{L}^*_{u_h}$ = adjoint of $\mathcal{L}_{u_h}$, 1/t
$l(\cdot)$ = linear form in the weak formulation
m_i = mass of the species i p.u. bulk volume, $\mathrm{m/L^3}$
N_e = number of elements, dimensionless
p = exponent in power law of relative permeability, dimensionless
p = fluid pressure, $\mathrm{m/Lt^2}$
p_α = pressure of the α-phase, $\mathrm{m/Lt^2}$
P_c = capillary pressure, $\mathrm{m/Lt^2}$
P_e = element Peclet number, dimensionless
q = distributed source term of u, 1/t
q_T = volumetric source of fluid p.u. bulk volume, $\mathrm{L^3/L^3}$
Q_i = distributed source term of species i, $\mathrm{m/L^3t}$
r = viscosity ratio, dimensionless
$\mathcal{R}(u_h)$ = grid-scale residual, 1/t
S_α = saturation of the α-phase, dimensionless
S^*_w = water saturation of the injected fluid, dimensionless
t = time, t
T = time interval, t
u = generic conserved quantity, dimensionless
u_h = grid-scale part of u, dimensionless
$\tilde{u}$ = subgrid-scale part of u, dimensionless
$\bar{u}$ = value of u for Dirichlet boundary conditions, dimensionless
u_0 = initial conditions of u, dimensionless
U_{sc} = characteristic value of u near a discontinuity, dimensionless
$\boldsymbol{v}_\alpha$ = velocity of the α-phase, L/t
$\boldsymbol{v}_T$ = total fluid velocity, L/t
$\mathcal{V}$ = space of trial functions
$\mathcal{V}_0$ = space of test functions
$\mathcal{V}_h$ = grid-scale space of trial functions
$\mathcal{V}_{h,0}$ = grid-scale space of test functions
$\tilde{\mathcal{V}}$ = space of subgrid scales
x, y = space coordinate, L

Greek letters

α_L = longitudinal dispersivity, L

$\Gamma_u =$ Dirichlet part of the boundary
$\Gamma_n =$ Neumann part of the boundary
$\delta =$ increment
$\lambda_\alpha =$ relative mobility of the α-phase, Lt/m
$\mu =$ dynamic viscosity of the mixture, m/Lt
$\mu_\alpha =$ dynamic viscosity of the α-phase, m/Lt
$\tilde{\Pi} =$ L^2-projection operator onto $\tilde{\mathcal{V}}$
$\rho =$ density of the mixture, m/L^3
$\rho_\alpha =$ density of the α-phase, m/L^3
$\tau =$ relaxation time, t
$\phi =$ porosity, dimensionless
$\Omega =$ spatial domain, L in 1D, L^2 in 2D, L^3 in 3D
$\partial\Omega =$ boundary of the domain

Subscripts
$o =$ oil
$s =$ tracer
$w =$ water

Superscripts
$(k) =$ iteration count

Acknowledgements

This work was supported by the U.S. Department of Energy under Contract No. DE-AC03-76SF00098. Funding provided by the Jane Lewis fellowship and the Repsol-YPF fellowship, awarded to the first author, is gratefully acknowledged.

References

[1] G. Chavent and J. Jaffré. *Mathematical Models and Finite Elements for Reservoir Simulation*, volume 17 of *Studies in Mathematics and its Applications*. Elsevier Science Pub., North-Holland, 1986.

[2] Z. Chen and R. E. Ewing. Comparison of various formulations of three-phase flow in porous media. *J. Comput. Phys.*, 132:362–373, 1997.

[3] F. Brezzi and M. Fortin. *Mixed and Hybrid Finite Element Methods*, volume 15 of *Springer Series in Computational Mathematics*. Springer-Verlag, New York, 1994.

[4] L. J. Durlofsky. Accuracy of mixed and control volume finite element approximations to darcy velocity and related quantities. *Water Resour. Res.*, 30(4):965–973, 1994.

[5] R. E. Ewing. Multidisciplinary interactions in energy and environmental modeling. *J. Comput. Appl. Math.*, 74:193–215, 1996.

[6] R. E. Ewing and H. Wang. A summary of numerical methods for time-dependent advection-dominated partial differential equations. *J. Comput. Appl. Math.*, 128:423–445, 2001.

[7] T. J. R. Hughes and A. N. Brooks. A multidimensional upwind scheme with no crosswind diffusion. In T. J. R. Hughes, editor, *Finite Element Methods for Convection Dominated Flows*, pages 19–35, New York, 1979. ASME.

[8] A. N. Brooks and T. J. R. Hughes. Streamline upwind Petrov-Galerkin formulations for convection dominated flows with particular emphasis on the incompressible Navier-Stokes equations. *Comput. Methods Appl. Mech. Engrg.*, 32:199–259, 1982.

[9] C. Johnson, U. Nävert, and J. Pitkäranta. Finite element methods for linear hyperbolic problems. *Comput. Methods Appl. Mech. Engrg.*, 45:285–312, 1984.

[10] R. Codina. A discontinuity-capturing crosswind-dissipation for the finite element solution of the convection-diffusion equation. *Comput. Methods Appl. Mech. Engrg.*, 110:325–342, 1993.

[11] E. G. Dutra do Carmo and A. C. Galeão. Feedback Petrov-Galerkin methods for convection-dominated problems. *Comput. Methods Appl. Mech. Engrg.*, 88:1–16, 1991.

[12] A. C. Galeão and E. G. Dutra do Carmo. A consistent approximate upwind Petrov-Galerkin method for convection-dominated problems. *Comput. Methods Appl. Mech. Engrg.*, 68:83–95, 1988.

[13] T. J. R. Hughes, M. Mallet, and A. Mizukami. A new finite element formulation for computational fluid dynamics: II. Beyond SUPG. *Comput. Methods Appl. Mech. Engrg.*, 54:341–355, 1986.

[14] T. J. R. Hughes and M. Mallet. A new finite element formulation for computational fluid dynamics: IV. A discontinuity-capturing operator for multidimensional advective-diffusive systems. *Comput. Methods Appl. Mech. Engrg.*, 58:329–336, 1986.

[15] C. Johnson. A new approach to algorithms for convection problems which are based on exact transport+projection. *Comput. Methods Appl. Mech. Engrg.*, 100:45–62, 1992.

[16] C. Johnson and A. Szepessy. On the convergence of a finite element method for a nonlinear hyperbolic conservation law. *Math. Comp.*, 49(180):427–444, 1987.

[17] C. Johnson, A. Szepessy, and P. Hansbo. On the convergence of shock-capturing streamline diffusion finite element methods for hyperbolic conservation laws. *Math. Comp.*, 54(189):107–129, 1990.

[18] T. E. Tezduyar and Y. J. Park. Discontinuity-capturing finite element formulations for nonlinear convection-diffusion-reaction equations. *Comput. Methods Appl. Mech. Engrg.*, 59:307–325, 1986.

[19] P. Colella. A direct Eulerian MUSCL scheme for gas dynamics. *SIAM J. Sci. Statist. Comput.*, 6(1):104–117, 1985.

[20] J. B. Goodman and R. J. LeVeque. A geometric approach to high-resolution TVD schemes. *SIAM J. Numer. Anal.*, 25(2):268–284, 1988.

[21] A. Harten. High resolution schemes for hyperbolic conservation laws. *J. Comput. Phys.*, 49(3):357–393, 1983.

[22] P. K. Sweby. High resolution schemes using flux limiters for hyperbolic conservation laws. *SIAM J. Numer. Anal.*, 21(5):995–1011, 1984.

[23] B. van Leer. Towards the ultimate conservative difference scheme. 2. Monotonicity and conservation combined in a second-order scheme. *J. Comput. Phys.*, 4(361–370), 14.

[24] A. Harten, B. Engquist, S. Osher, and S. Chakravarthy. Uniformly high-order accurate essentially nonoscillatory schemes, III. *J. Comput. Phys.*, 71:231–241, 1987.

[25] C.-W. Shu. Essentially nonoscillatory (ENO) and weighted essentially nonoscillatory (WENO) schemes for hyperbolic conservation laws. In A. Quarteroni, editor, *Advanced Numerical Approximation of Nonlinear Hyperbolic Equations*, volume 1697 of *Lecture Notes in Mathematics*, pages 325–432. Springer-Verlag, New York, 1997.

[26] C. Johnson and J. Pitkäranta. An analysis of discontinuous Galerkin methods for a scalar hyperbolic equation. *Math. Comp.*, 46:1–26, 1986.

[27] B. Cockburn. Finite element methods for conservation laws. *J. Comput. Appl. Math.*, 128:187–204, 2001.

[28] C. L. Farmer. A moving point method for arbitrary Peclet number multi-dimensional convection-diffusion equations. *IMA J. Numer. Anal.*, 5:465–480, 1980.

[29] A. O. Garder, D. W. Peaceman, and A. L. Pozzi. Numerical calculations of multidimensional miscible displacement by the method of characteristics. *Soc. Pet. Eng. J.*, 4(1):26–36, 1964.

[30] J. Douglas Jr. and T. F. Russell. Numerical methods for convection-dominated diffusion problems based on combining the method of characteristics with finite element or finite difference procedures. *SIAM J. Numer. Anal.*, 19:871–885, 1982.

[31] O. Pironneau. On the transport-diffusion algorithm and its application to the Navier-Stokes equations. *Numer. Math.*, 38:309–332, 1982.

[32] G. Thomaidis, K. Zygourakis, and M. F. Wheeler. An explicit finite difference scheme based on the modified method of characteristics for solving diffusion-convection problems in one space dimension. *Numer. Methods Partial Differential Equations*, 4:119–138, 1988.

[33] S. P. Neuman. An Eulerian-Lagrangian numerical scheme for the dispersion-convection equation using conjugate space-time grids. *J. Comput. Phys.*, 41:270–294, 1981.

[34] S. P. Neuman. Adaptive Eulerian-Lagrangian finite element method for advection-dispersion equation. *Int. J. Numer. Meth. Engrg.*, 20:321–337, 1984.

[35] M. A. Celia, T. F. Russell, I. Herrera, and R. E. Ewing. An Eulerian-Lagrangian localized adjoint method for the advection-diffusion equation. *Adv. Water Resour.*, 13(4):187–206, 1990.

[36] I. Herrera, R. E. Ewing, M. A. Celia, and T. F. Russell. Eulerian-Lagrangian localized adjoint methods: the theoretical framework. *Numer. Methods Partial Differential Equations*, 9:431–458, 1993.

[37] H. K. Dahle, R. E. Ewing, and T. F. Russell. Eulerian-Lagrangian localized adjoint methods for a nonlinear advection-diffusion equation. *Comput. Methods Appl. Mech. Engrg.*, 122:223–250, 1995.

[38] P. J. Binning and M. A. Celia. A finite volume Eulerian-Lagrangian localized adjoint method for solution of the contaminant transport equations in two-dimensional multi-phase systems. *Water Resour. Res.*, 32(1):103–114, 1996.

[39] H. Wang, H. K. Dahle, R. E. Ewing, M. S. Espedal, R. C. Sharpley, and S. Man. An ELLAM scheme for advection-diffusion equations in two dimensions. *SIAM J. Sci. Comput.*, 20:2160–2194, 1999.

[40] H. Wang, R. E. Ewing, G. Qin, S. L. Lyons, M. Al-Lawatia, and S. Man. A family of Eulerian-Lagrangian localized adjoint methods for multi-dimensional advection-reaction equations. *J. Comput. Phys.*, 152:120–163, 1999.

[41] T. J. R. Hughes, L. P. Franca, and G. M. Hulbert. A new finite element formulation for computational fluid dynamics: VIII. The Galerkin least-squares method for advective-diffusive equations. *Comput. Methods Appl. Mech. Engrg.*, 73:173–189, 1989.

[42] L. P. Franca, S. L. Frey, and T. J. R. Hughes. Stabilized finite element methods: I. Application to the advective-diffusive model. *Comput. Methods Appl. Mech. Engrg.*, 95:253–276, 1992.

[43] T. J. R. Hughes. Multiscale phenomena: Green's functions, the Dirichlet-to-Neumann formulation, subgrid scale models, bubbles and the origins of stabilized methods. *Comput. Methods Appl. Mech. Engrg.*, 127:387–401, 1995.

[44] T. J. R. Hughes, G. R. Feijóo, L. Mazzei, and J.-B. Quincy. The variational multiscale method—a paradigm for computational mechanics. *Comput. Methods Appl. Mech. Engrg.*, 166:3–24, 1998.

[45] R. Codina. Comparison of some finite element methods for solving the diffusion-convection-reaction equation. *Comput. Methods Appl. Mech. Engrg.*, 156:185–210, 1998.

[46] K. Aziz and A. Settari. *Petroleum Reservoir Simulation*. Elsevier Science Pub., London, 1979.

[47] D. W. Peaceman. *Fundamentals of Numerical Reservoir Simulation*, volume 6 of *Developments in Petroleum Science*. Elsevier Science Pub., Amsterdam, 1977.

[48] J. Bear. *Dynamics of Fluids in Porous Media*. Environmental Science Series. American Elsevier Pub. Co., New York, 1972. Reprinted with corrections, Dover Pub., New York, 1988.

[49] G. Chavent and J. E. Roberts. A unified physical presentation of mixed, mixed-hybrid finite elements and standard finite difference approximations for the determination of velocities in waterflow problems. *Adv. Water Resour.*, 14(6):329–348, 1991.

[50] R. E. Ewing. Simulation of multiphase flows in porous media. *Transport in Porous Media*, 6:479–499, 1991.

[51] E. F. Kaasschieter. Mixed finite elements for accurate particle tracking in saturated groundwater flow. *Adv. Water Resour.*, 18(5):277–294, 1995.

[52] L. Bergamaschi, S. Mantica, and G. Manzini. A mixed finite element–finite volume formulation of the black-oil model. *SIAM J. Sci. Comput.*, 20(3):970–997, 1998.

[53] R. Codina. Stabilized finite element approximation of transient incompressible flows using orthogonal subscales. *Comput. Methods Appl. Mech. Engrg.*, 2001. (Submitted).

[54] R. Codina. On stabilized finite element methods for linear systems of convection-diffusion-reaction equations. *Comput. Methods Appl. Mech. Engrg.*, 188:61–82, 2000.

[55] R. J. LeVeque. *Numerical Methods for Conservation Laws*. Birkhäuser Verlag, Berlin, second edition, 1992.

[56] K. Garikipati and T. J. R. Hughes. A study of strain localization in a multiple scale framework—The one-dimensional problem. *Comput. Methods Appl. Mech. Engrg.*, 159:193–222, 1998.

[57] S. E. Buckley and M. C. Leverett. Mechanism of fluid displacement in sands. *Trans. SPE of AIME*, 146:107, 1942.

[58] M. R. Todd, P. M. O'Dell, and G. J. Hirasaki. Methods of increased accuracy in numerical reservoir simulators. *Trans. SPE of AIME*, 253:515–530, December 1972. (SPEJ).

[59] A. Settari and K. Aziz. Treatment of nonlinear terms in the numerical solution of partial differential equations for multiphase flow in porous media. *Int. J. Multiphase Flow*, 1:817–844, 1975.

[60] P. Binning and M. A. Celia. Practical implementation of the fractional flow approach to multi-phase flow simulation. *Adv. Water Resour.*, 22(5):461–478, 1999.

[61] K. E. Jansen, S. S. Collis, C. Whiting, and F. Shakib. A better consistency for low-order stabilized finite element methods. *Comput. Methods Appl. Mech. Engrg.*, 174:153–170, 1999.

[62] R. Codina and J. Blasco. Analysis of a stabilized finite element approximation of the transient convection-diffusion-reaction equation using orthogonal subscales. *Comput. Visual. Sci.*, 2001. (Submitted).

[63] C. Baiocchi, F. Brezzi, and L. P. Franca. Virtual bubbles and Galerkin/least-squares type methods (Ga.L.S). *Comput. Methods Appl. Mech. Engrg.*, 105:125–141, 1993.

[64] L. P. Franca, A. Nesliturk, and M. Stynes. On the stability of residual free bubbles for convection-diffusion problems and their approximation by a two-level finite element method. *Comput. Methods Appl. Mech. Engrg.*, 166:35–49, 1998.

[65] C. Canuto and V. van Kemenade. Bubble-stabilized spectral methods for the incompressible Navier-Stokes equations. *Comput. Methods Appl. Mech. Engrg.*, 135:35–61, 1996.

[66] J.-L. Guermond. Stabilization of Galerkin approximations of transport equations by subgrid modeling. *Mathematical Modeling and Numerical Analysis*, 33:1293–1316, 1999.

[67] J.-L. Guermond. Subgrid stabilization of Galerkin approximations of linear contraction semi-groups of class C^0 in Hilbert spaces. *Numer. Methods Partial Differential Equations*, 17(1):1–25, 2001.

[68] A. A. O. Ammi and M. Marion. Nonlinear Galerkin methods and mixed finite elements: two-grid algorithms for the Navier-Stokes equations. *Numer. Math.*, 68:189–213, 1994.

[69] J. B. Burie and M. Marion. Multilevel methods in space and time for the Navier-Stokes equations. *SIAM J. Numer. Anal.*, 34:1574–1599, 1997.